First observation of $\psi(2S) \to p\bar{n}\pi^- + c.c.$

M. Ablikim[1], J. Z. Bai[1], Y. Ban[12], J. G. Bian[1], X. Cai[1], H. F. Chen[17], H. S. Chen[1], H. X. Chen[1], J. C. Chen[1], Jin Chen[1], Y. B. Chen[1], S. P. Chi[2], Y. P. Chu[1], X. Z. Cui[1], Y. S. Dai[19], L. Y. Diao[9], Z. Y. Deng[1], Q. F. Dong[15], S. X. Du[1], J. Fang[1], S. S. Fang[2], C. D. Fu[1], C. S. Gao[1], Y. N. Gao[15], S. D. Gu[1], Y. T. Gu[4], Y. N. Guo[1], Y. Q. Guo[1], Z. J. Guo[16], F. A. Harris[16], K. L. He[1], M. He[13], Y. K. Heng[1], H. M. Hu[1], T. Hu[1], G. S. Huang[1a], X. T. Huang[13], X. B. Ji[1], X. S. Jiang[1], X. Y. Jiang[5], J. B. Jiao[13], D. P. Jin[1], S. Jin[1], Yi Jin[8], Y. F. Lai[1], G. Li[2], H. B. Li[1], H. H. Li[1], J. Li[1], R. Y. Li[1], S. M. Li[1], W. D. Li[1], W. G. Li[1], X. L. Li[1], X. N. Li[1], X. Q. Li[11], Y. L. Li[4], Y. F. Liang[14], H. B. Liao[1], B. J. Liu[1], C. X. Liu[1], F. Liu[6], Fang Liu[1], H. H. Liu[1], H. M. Liu[1], J. Liu[12], J. B. Liu[1], J. P. Liu[18], Q. Liu[1], R. G. Liu[1], Z. A. Liu[1], Y. C. Lou[5], F. Lu[1], G. R. Lu[5], J. G. Lu[1], C. L. Luo[10], F. C. Ma[9], H. L. Ma[1], L. L. Ma[1], Q. M. Ma[1], X. B. Ma[5], Z. P. Mao[1], X. H. Mo[1], J. Nie[1], S. L. Olsen[16], H. P. Peng[17b], R. G. Ping[1], N. D. Qi[1], H. Qin[1], J. F. Qiu[1], Z. Y. Ren[1], G. Rong[1], L. Y. Shan[1], L. Shang[1], C. P. Shen[1], D. L. Shen[1], X. Y. Shen[1], H. Y. Sheng[1], H. S. Sun[1], J. F. Sun[1], S. S. Sun[1], Y. Z. Sun[1], Z. J. Sun[1], Z. Q. Tan[4], X. Tang[1], G. L. Tong[1], G. S. Varner[16], D. Y. Wang[1], L. Wang[1], L. L. Wang[1], L. S. Wang[1], M. Wang[1], P. Wang[1], P. L. Wang[1], W. F. Wang[1c], Y. F. Wang[1], Z. Wang[1], Z. Y. Wang[1], Zhe Wang[1], Zheng Wang[2], C. L. Wei[1], D. H. Wei[1], N. Wu[1], X. M. Xia[1], X. X. Xie[1], G. F. Xu[1], X. P. Xu[6], Y. Xu[11], M. L. Yan[17], H. X. Yang[1], Y. X. Yang[3], M. H. Ye[2], Y. X. Ye[17], Z. Y. Yi[1], G. W. Yu[1], C. Z. Yuan[1], J. M. Yuan[1], Y. Yuan[1], S. L. Zang[1], Y. Zeng[7], Yu Zeng[1], B. X. Zhang[1], B. Y. Zhang[1], C. C. Zhang[1], D. H. Zhang[1], H. Q. Zhang[1], H. Y. Zhang[1], J. W. Zhang[1], J. Y. Zhang[1], S. H. Zhang[1], X. M. Zhang[1], X. Y. Zhang[13], Yiyun Zhang[14], Z. P. Zhang[17], D. X. Zhao[1], J. W. Zhao[1], M. G. Zhao[1], P. P. Zhao[1], W. R. Zhao[1], Z. G. Zhao[1d], H. Q. Zheng[12], J. P. Zheng[1], Z. P. Zheng[1], L. Zhou[1], N. F. Zhou[1c], K. J. Zhu[1], Q. M. Zhu[1], Y. C. Zhu[1], Y. S. Zhu[1], Yingchun Zhu[1b], Z. A. Zhu[1], B. A. Zhuang[1], X. A. Zhuang[1], B. S. Zou[1]

(BES Collaboration)

[1] *Institute of High Energy Physics, Beijing 100049, People's Republic of China*

[2] *China Center for Advanced Science and Technology*

(CCAST), Beijing 100080, People's Republic of China

[3] *Guangxi Normal University, Guilin 541004, People's Republic of China*

[4] *Guangxi University, Nanning 530004, People's Republic of China*

[5] *Henan Normal University, Xinxiang 453002, People's Republic of China*

[6] *Huazhong Normal University, Wuhan 430079, People's Republic of China*

[7] *Hunan University, Changsha 410082, People's Republic of China*

[8] *Jinan University, Jinan 250022, People's Republic of China*

[9] *Liaoning University, Shenyang 110036, People's Republic of China*

[10] *Nanjing Normal University, Nanjing 210097, People's Republic of China*

[11] *Nankai University, Tianjin 300071, People's Republic of China*

[12] *Peking University, Beijing 100871, People's Republic of China*

[13] *Shandong University, Jinan 250100, People's Republic of China*

[14] *Sichuan University, Chengdu 610064, People's Republic of China*

[15] *Tsinghua University, Beijing 100084, People's Republic of China*

[16] *University of Hawaii, Honolulu, HI 96822, USA*

[17] *University of Science and Technology of China, Hefei 230026, People's Republic of China*

[18] *Wuhan University, Wuhan 430072, People's Republic of China*

[19] *Zhejiang University, Hangzhou 310028, People's Republic of China*

[a] *Current address: Purdue University, West Lafayette, IN 47907, USA*

[b] *Current address: DESY, D-22607, Hamburg, Germany*

[c] *Current address: Laboratoire de l'Accélérateur Linéaire, Orsay, F-91898, France*

[d] *Current address: University of Michigan, Ann Arbor, MI 48109, USA*

Abstract

Using 14 million $\psi(2S)$ events collected with the Beijing Spectrometer (BESII) at the Beijing Electron-Positron Collider, the branching fractions of $\psi(2S)$ decays to $p\bar{n}\pi^-$ and $\bar{p}n\pi^+$ and the branching fractions of the main background channels $\psi(2S) \to p\bar{n}\pi^-\pi^0$, $\psi(2S) \to \gamma\chi_{c0} \to \gamma p\bar{n}\pi^-$, $\psi(2S) \to \gamma\chi_{c2} \to \gamma p\bar{n}\pi^-$, and $\psi(2S) \to \gamma\chi_{cJ} \to \gamma p\bar{n}\pi^-\pi^0$ are determined. The contributions of the N^* resonances in $\psi(2S) \to p\bar{n}\pi^- + c.c.$ are also discussed.

PACS numbers: 14.20.Gk, 13.75.Gx, 13.25.Gv

I. INTRODUCTION

From perturbative QCD (pQCD), it is expected that both J/ψ and $\psi(2S)$ decaying into light hadrons are dominated by the annihilation of $c\bar{c}$ into three gluons, with widths proportional to the square of the wave function at the origin $|\Psi(0)|^2$ [1]. This yields the pQCD "12% rule"

$$Q_h = \frac{B_{\psi(2S)\to h}}{B_{J/\psi\to h}} \approx \frac{B_{\psi(2S)\to e^+e^-}}{B_{J/\psi\to e^+e^-}} \approx 12\%.$$

The violation of this rule was first observed in the $\rho\pi$ and $K^{*+}K^- + c.c.$ decay modes by Mark-II [2]. Following the scenario proposed in Ref. [3], that the small $\psi(2S) \to \rho\pi$ branching fraction is due to the cancellation of the S- and D-wave matrix elements in $\psi(2S)$ decays, it was suggested that all $\psi(2S)$ decay channels should be affected by the same S- and D-wave mixing scheme, and thus all ratios of branching fractions of $\psi(2S)$ and J/ψ decays into the same final state could have values different from 12%, expected between pure $1S$ and $2S$ states [4]. The mixing scenario also predicts $\psi(3770)$ decay branching fractions since the $\psi(3770)$ is a mixture of S- and D-wave charmonia, as well. Many channels of J/ψ, $\psi(2S)$, and $\psi(3770)$ decays should be measured to test this scenario.

A very important source of information on nucleon internal structure is the N^* mass spectrum, including production and decay rates. Because of its importance for the understanding of nonperturbative QCD, a series of experiments on N^* physics with electromagnetic probes (real photons and electrons with space-like virtual photons) are being performed at facilities such as JLAB, ELSA at Bonn, GRAAL at Grenoble, and SPRING8 at JASRI [5]. They have already produced some results [6, 7]. However, our knowledge on N^* resonances is still poor. Even for the well-established lowest excited state, the $N^*(1440)$, properties such as mass, width, and decay branching fractions still have large experimental uncertainties [8]. Another outstanding problem is that, in many of its forms, the quark model predicts a substantial number of N^* states around 2 GeV/c^2, which have not yet been observed [9].

Recent studies of N^* resonances have been performed using J/ψ events collected at the Beijing Electron-Positron Collider (BEPC) [10, 11], providing a new method for probing this physics, and a new N^* peak with a mass at around 2065 MeV/c^2 was observed [11]. This may be one of the "missing" N^* states around 2 GeV/c^2. However, due to its large mass, the production of this $N^*(2065)$ in J/ψ decays is rather limited in phase space. A similar search for it in $\psi(2S) \to p\bar{p}\pi^0$ has been performed [12], where there is a faint but not

statistically significant accumulation of events in the $p\pi$ invariant mass spectrum at around 2065 MeV/c^2.

In this paper, we study $\psi(2S) \to p\bar{n}\pi^- + c.c.$ and their main background channels, determine branching fractions, test the 12% rule, and study N^* resonances in the $N\pi$ system.

II. BES DETECTOR AND THE DATA SAMPLE

BESII is a large solid-angle magnetic spectrometer which is described in detail in Ref. [13]. The momentum of charged particles is determined by a 40-layer cylindrical main drift chamber (MDC) which has a momentum resolution of σ_p/p=1.7%$\sqrt{1+p^2}$ (p in GeV/c). Particle identification (PID) is accomplished using specific ionization (dE/dx) measurements in the drift chamber and time-of-flight (TOF) information in a barrel-like array of 48 scintillation counters. The dE/dx resolution is $\sigma_{dE/dx} \simeq 8.0\%$; the TOF resolution for Bhabha events is $\sigma_{TOF} = 180$ ps. Radially outside of the time-of-flight counters is a 12-radiation-length barrel shower counter (BSC) comprised of gas tubes interleaved with lead sheets. The BSC measures the energy and direction of photons with resolutions of $\sigma_E/E \simeq 21\%/\sqrt{E}$ (E in GeV), $\sigma_\phi = 7.9$ mrad, and $\sigma_z = 2.3$ cm. The iron flux return of the magnet is instrumented with three double layers of proportional counters (MUC) that are used to identify muons.

In the analysis, a GEANT3-based Monte Carlo (MC) simulation program (SIMBES) with detailed consideration of the detector performance is used. The consistency between data and Monte Carlo has been checked in many high purity physics channels, and the agreement is reasonable [14]. For the MC generators, the angular distribution for $\psi(2S) \to \gamma\chi_{cJ}$ is simulated assuming a pure $E1$ transition, and uniform phase space is used for the other decays.

The data sample used for this analysis consists of $(14.0 \pm 0.6) \times 10^6$ $\psi(2S)$ events taken at $\sqrt{s} = 3.686$ GeV [15]. Backgrounds are estimated using an inclusive $\psi(2S)$ decay MC sample generated by LUNDCRM [16] with the same size as the $\psi(2S)$ data.

III. EVENT SELECTION

For the signal channel $\psi(2S) \to p\bar{n}\pi^- + c.c.$ and the background channels, we reconstruct two charged tracks, and the neutron and antineutron are not measured. However, since

most antineutrons annihilate in the detector (mainly in the BSC) and most neutrons pass through the detector without interaction, these signatures are used to suppress backgrounds by requiring a neutral cluster in the expected antineutron direction and requiring nothing in the neutron direction.

A neutral cluster is considered to be a good photon candidate if the following requirements are satisfied: it is located within the BSC fiducial region; the energy deposited in the BSC is greater than 50 MeV; the first hit appears in the first 6 radiation lengths; the angle between the cluster development direction in the BSC and the photon emission direction from the beam interaction point (IP) is less than 37°; and the angle between the cluster and the nearest charged particle is greater than 15°.

Each charged track is required to be well fit by a three dimensional helix, to originate from the interaction point, $V_{xy} = \sqrt{V_x^2 + V_y^2} < 1$ cm, $|V_z| < 15$ cm, and to have a polar angle $|\cos\theta| < 0.8$. Here V_x, V_y, and V_z are the x, y, and z coordinates of the point of closest approach to the beam axis. The TOF and dE/dx measurements for each charged track are used to calculate $\chi^2_{PID}(i)$ values and the corresponding confidence levels $Prob_{PID}(i)$ for the hypotheses that a track is a pion, kaon, or proton, where i ($i = \pi/K/p$) is the particle type.

We use the following common selection criteria for all channels:

1. The number of charged tracks in the MDC is two with net charge zero, and the difference in V_z between the positive and negative charged tracks $|V_z^+ - V_z^-|$ is required to be less than 3 cm.

2. For each charged track, the particle identification confidence level for a candidate particle assignment is required to be greater than 0.01. For a proton we also require $Prob_{PID}(p) > Prob_{PID}(\pi)$ and $Prob_{PID}(p) > Prob_{PID}(K)$, and for a π, we require $Prob_{PID}(\pi) > Prob_{PID}(p)$ and $Prob_{PID}(\pi) > Prob_{PID}(K)$.

3. The energy of the positive charged track observed in the BSC should be less than 0.7 GeV in order to eliminate $\psi(2S) \to e^+e^-$ and Bhabha events.

4. $M_{p\pi^-(\text{or } \bar{p}\pi^+)} > 1.15$ GeV/c^2 to remove background channels with Λ or $\bar{\Lambda}$.

For $\psi(2S) \to p\bar{n}\pi^- + c.c.$ when there are photon candidates in the events, $\alpha < 10°$ is required, where α is the angle between the nearest neutral cluster and the missing momentum direction of the two charged tracks. When there are no photon candidates in an event, the

value of α is set to zero degree. After all above requirements, we obtain the $p\pi^-$ and $\bar{p}\pi^+$ missing mass distributions shown in Fig. 1, where there are clear signals of n and $\bar{n}$ at around 0.94 GeV/c^2. The background level increases from about 10 events per 20 MeV/c^2 bin at 0.6 GeV/c^2 to about 30 events at about 1.2 GeV/c^2.

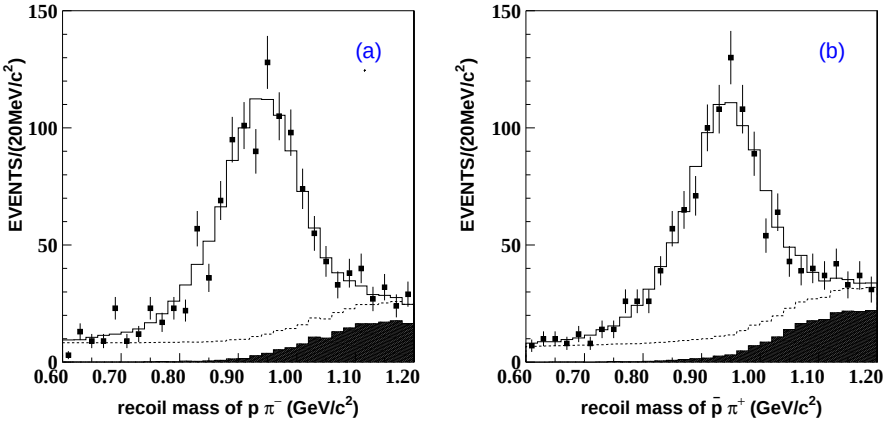

FIG. 1: Missing mass distributions of (a) $p\pi^-$ and (b) $\bar{p}\pi^+$ of $\psi(2S) \to p\bar{n}\pi^- + c.c.$ candidate events. The squares with error bars are data, the blank histograms are the fit, the shaded histograms are normalized backgrounds from $\psi(2S) \to \gamma\chi_{cJ}, \chi_{cJ} \to p\bar{n}\pi^- + c.c.$, $\psi(2S) \to p\bar{n}\pi^-\pi^0 + c.c.$, $\psi(2S) \to \gamma\chi_{cJ}, \chi_{cJ} \to p\bar{n}\pi^-\pi^0 + c.c.$, and the dashed curves are background shapes from the fit.

IV. BACKGROUND ANALYSIS

Backgrounds are studied using the $\psi(2S)$ inclusive decay MC sample. By applying the same selection criteria, it is found that for $\psi(2S) \to p\bar{n}\pi^-$ the main backgrounds are from $\psi(2S) \to \gamma\chi_{cJ}, \chi_{cJ} \to p\bar{n}\pi^-\pi^0$, $\psi(2S) \to p\bar{n}\pi^-\pi^0$, and $\psi(2S) \to \gamma\chi_{cJ}, \chi_{cJ} \to p\bar{n}\pi^-$. All these modes have not been measured previously. Here we measure these channels.

For these three background channels, in addition to the above selection criteria, we also require:

1. For $\psi(2S) \to \gamma\chi_{cJ}, \chi_{cJ} \to p\bar{n}\pi^-\pi^0$ events, we do a one-constraint (1C) kinematic fit to $\psi(2S) \to \gamma\gamma\gamma p\bar{n}\pi^-$ looping over all photon candidates. The combination with the minimum χ^2 is selected, and $Prob_{1C} > 0.01$ is required. After the 1C fit, the direction of the $\bar{n}$ is determined. Similar requirements are imposed on $\psi(2S) \to \gamma\gamma p\bar{n}\pi^-$ and

$\psi(2S) \to \gamma p\bar{n}\pi^-$ final states in selecting $\psi(2S) \to p\bar{n}\pi^-\pi^0$ and $\psi(2S) \to \gamma\chi_{cJ}, \chi_{cJ} \to p\bar{n}\pi^-$.

2. The angle between the direction of $\bar{n}$ and one of the neutral clusters not already used in the kinematic fit should be less than ten degrees.

A. $\psi(2S) \to \gamma\chi_{cJ}, \chi_{cJ} \to p\bar{n}\pi^-\pi^0$

For this channel, we require four photon candidates (three of them from the radiative and π^0 decays, the other from the interaction between the antineutron and the detector material) and the angle between the two photons from π^0 decays be greater than eight degrees to remove the background from split-off fake photons. In order to suppress the background from $\psi(2S) \to \pi^0\pi^0 J/\psi, J/\psi \to p\bar{n}\pi^-$, the requirement $|m_{p\bar{n}\pi^-} - 3.097| > 0.05$ GeV/c^2 is used. After applying the above selection criteria, the $\gamma\gamma$ invariant mass spectrum, shown in Fig. 2, is obtained, and $|m_{\gamma\gamma} - 0.135| < 0.03$ GeV/c^2 is required to select π^0 candidates.

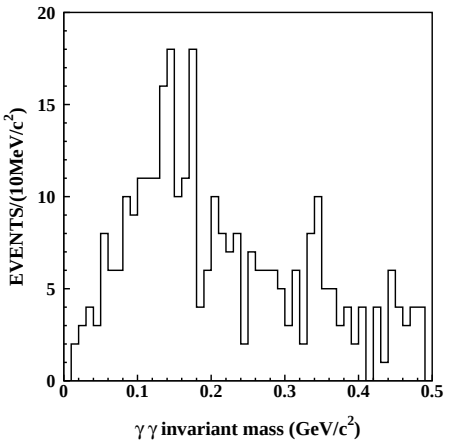

FIG. 2: The $\gamma\gamma$ invariant mass distribution for selected $\psi(2S) \to \gamma p\bar{n}\pi^-\gamma\gamma$ candidate events.

The $p\bar{n}\pi^-\gamma\gamma$ invariant mass distribution for the selected $\psi(2S) \to \gamma p\bar{n}\pi^-\pi^0$ candidate events is shown in Fig. 3. The shaded histogram shows the main backgrounds from $\psi(2S) \to \pi^0\pi^0 J/\psi, J/\psi \to p\bar{n}\pi^-$ and $\psi(2S) \to p\bar{n}\pi^-\pi^0$, which have been normalized to data using the branching fractions of $J/\psi \to p\bar{n}\pi^-$ and $\psi(2S) \to p\bar{n}\pi^-\pi^0$ from Ref. [11] and our measurements (see Sec. IV B). From Fig. 3, no clear χ_{cJ} signals are seen. Since the

background in this channel is very complicated, we set an upper limit for $\chi_{cJ} \to p\bar{n}\pi^-\pi^0$ by subtracting the known backgrounds from the total number of observed events and obtain 45 ± 9 events for $p\bar{n}\pi^-\pi^0$ invariant mass greater than 3.2 GeV/c^2. Assuming a Gaussian distribution, the upper limit at the 90% C. L. is 57. Using the MC simulated efficiency ϵ_1 of $(4.00 \pm 0.09)\%$, we obtain:

$$\sum_{J=0}^{2} B(\psi(2S) \to \gamma\chi_{cJ}, \chi_{cJ} \to p\bar{n}\pi^-\pi^0) < \frac{N^{up}_{\gamma p\bar{n}\pi^-\pi^0}}{N_{\psi(2S)} \cdot \epsilon_1 \cdot f_1 \cdot f_3 \cdot (1-s) \cdot B(\pi^0 \to \gamma\gamma)} = 1.2{\times}10^{-4},$$

at the 90% C. L. Here f_1 and f_3 are efficiency correction factors (see Sec. V, items 6 and 8) and s is the systematic error (see Table I).

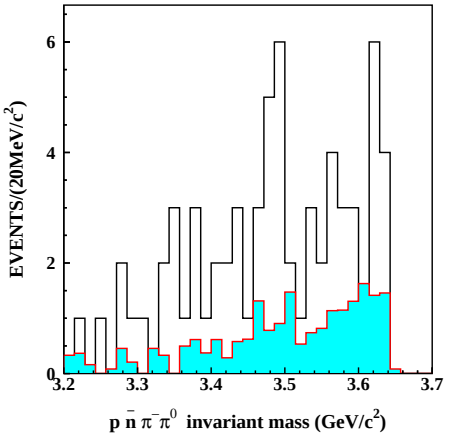

FIG. 3: The $p\bar{n}\pi^-\gamma\gamma$ invariant mass distribution for selected $\psi(2S) \to \gamma p\bar{n}\pi^-\pi^0$ candidate events. The shaded histogram is the sum of $\psi(2S) \to \pi^0\pi^0 J/\psi, J/\psi \to p\bar{n}\pi^-$ and $\psi(2S) \to p\bar{n}\pi^-\pi^0$ backgrounds which have been normalized to data according to their branching fractions.

B. $\psi(2S) \to p\bar{n}\pi^-\pi^0$

For this channel, we require the number of selected photon candidates equals three (two of them come from π^0 decays and the other from the interaction of the antineutron with the detector material) and the angle between the two photons from π^0 decays be greater than eight degrees to remove the background from split-off fake photons. The $\gamma\gamma$ invariant mass distribution after applying all the above selection criteria is shown in Fig. 4, where a clear π^0

signal can be seen. From the exclusive MC simulation, it is seen that possible backgrounds, except $\psi(2S) \to \gamma\chi_{cJ}, \chi_{cJ} \to p\bar{n}\pi^-\pi^0$, have no peak at the π^0 mass in the $\gamma\gamma$ invariant mass distributions, and therefore they will not contribute to the number of π^0 events in fitting the $\gamma\gamma$ invariant mass distribution. For $\psi(2S) \to \gamma\chi_{cJ}, \chi_{cJ} \to p\bar{n}\pi^-\pi^0$ background, after normalizing to data according to the branching fraction measured above, the contribution of this background is so small that it can be neglected.

By fitting the $\gamma\gamma$ invariant mass spectrum with a MC determined signal shape and a 2nd order Legendre polynomial for background, as shown in Fig. 4, 135 ± 21 $\psi(2S) \to p\bar{n}\pi^-\pi^0$ candidate events are obtained. The statistical significance is 8.1σ, and the detection efficiency ϵ_2 for this decay mode is $(3.21 \pm 0.08)\%$. We obtain:

$$B(\psi(2S) \to p\bar{n}\pi^-\pi^0) = \frac{N^{sig}_{p\bar{n}\pi^-\pi^0}}{N_{\psi(2S)} \cdot \epsilon_2 \cdot f_1 \cdot f_3 \cdot B(\pi^0 \to \gamma\gamma)} = (3.18 \pm 0.50) \times 10^{-4},$$

where f_1, f_3 are the efficiency correction factors, and the error is statistical.

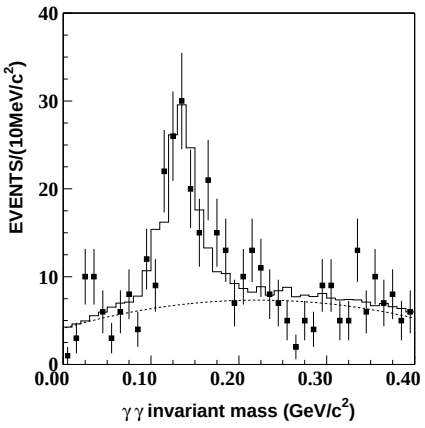

FIG. 4: The $\gamma\gamma$ invariant mass distribution of the selected $\psi(2S) \to \gamma\gamma p\bar{n}\pi^-$ candidate events. The squares with error bars are data, and the histogram is the fit.

C. $\psi(2S) \to \gamma\chi_{cJ}, \chi_{cJ} \to p\bar{n}\pi^-$

For this channel, we require two photon candidates (one comes from radiative decay and the other one from the interaction between the antineutron and the detector material). After applying all the above selection criteria, the $p\bar{n}\pi^-$ invariant mass distribution, shown in

Fig. 5, is obtained. Here χ_{c0} and χ_{c2} signals can be seen, but the χ_{c1} signal is less significant. In fitting, we neglect the χ_{c1} signal, and 85 ± 18 and 80 ± 16 events are obtained by fitting the $p\bar{n}\pi^-$ invariant mass spectrum with MC simulated χ_{c0} and χ_{c2} signal histograms and a background shape. Here the background shape includes a 2nd order Legendre function and a normalized histogram obtained from background channel $\psi(2S) \to p\bar{n}\pi^-$ measured in this work.

The statistical significance of χ_{c0} and χ_{c2} are both 4.2σ, and the detection efficiencies for χ_{c0} (ϵ_3) and χ_{c2} (ϵ_4) are $(5.77 \pm 0.11)\%$ and $(6.14 \pm 0.11)\%$, respectively. We obtain:

$$B(\psi(2S) \to \gamma\chi_{c0}, \chi_{c0} \to p\bar{n}\pi^-) = \frac{N^{sig}_{\chi_{c0}\to p\bar{n}\pi^-}}{N_{\psi(2S)} \cdot \epsilon_3 \cdot f_1 \cdot f_3} = (1.10 \pm 0.24) \times 10^{-4},$$

$$B(\psi(2S) \to \gamma\chi_{c2}, \chi_{c2} \to p\bar{n}\pi^-) = \frac{N^{sig}_{\chi_{c2}\to p\bar{n}\pi^-}}{N_{\psi(2S)} \cdot \epsilon_4 \cdot f_1 \cdot f_3} = (0.97 \pm 0.20) \times 10^{-4},$$

where f_1 and f_3 are the efficiency correction factors, and the errors are statistical.

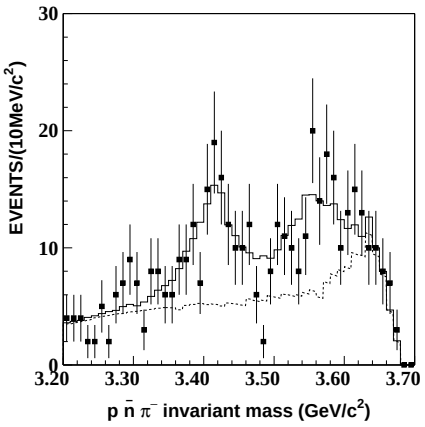

FIG. 5: The $p\bar{n}\pi^-$ invariant mass distribution of the selected $\psi(2S) \to \gamma p\bar{n}\pi^-$ candidate events. The squares with error bars are data, the histogram is the fit, and the dashed curve is the background shape from the fit.

Since the neutron passes through the detector without interaction in almost all cases, the background level will be higher and more complicated than for the antineutron final state, so we do not try to measure the charge conjugate modes of the above three channels. In the following analysis, we assume the branching fractions for these three channels equal to their charge conjugate modes.

V. SYSTEMATIC ERRORS

Systematic errors in measuring the branching fractions mainly originate from the MC statistics, the error matrix of the track finding and the 1C kinematic fit, the vertex requirement, particle identification, the photon efficiency, the α selection criterion, the total number of $\psi(2S)$ events, and the fitting of the signal.

1. The MDC tracking efficiency was measured using channels like $J/\psi \to \Lambda\bar{\Lambda}$ and $\psi(2S) \to \pi^+\pi^- J/\psi, J/\psi \to \mu^+\mu^-$. It is found that the MC simulation agrees with data within $(1-2)\%$ for each charged track. Therefore, 4% is taken as the systematic error for events with two charged tracks.

2. The difference in V_z between the positive and negative charged tracks $|V_z^+ - V_z^-|$ is required to be less than 3 cm, this corresponds to an about three-standard-deviation requirement. The effect of it is checked with $J/\psi \to p\bar{n}\pi^- + c.c.$ candidate events, it is found that MC simulates data within 0.6%. This is taken as systematic error of this selection criterion.

3. The photon detection efficiency was studied with different methods using $J/\psi \to \pi^+\pi^-\pi^0$ events [14], and the difference between data and MC simulation is about 2% for each photon. We take 2% per photon in the analysis.

4. Particle identification is used in selecting candidate events, and we take 5% as the systematic error [11].

5. The systematic error from the 1C kinematic fit should be smaller than for the 4C kinematic fit, since there are fewer constraints. Various studies show that the uncertainty of the 4C kinematic fit is around 4% [17], so here we conservatively take 4% as the error from the 1C kinematic fit.

6. The uncertainties of background shapes in $\psi(2S) \to p\bar{n}\pi^-$, $\psi(2S) \to \bar{p}n\pi^+$, $\psi(2S) \to p\bar{n}\pi^-\pi^0 + c.c.$, $\psi(2S) \to \gamma\chi_{c0}, \chi_{c0} \to p\bar{n}\pi^-$, and $\psi(2S) \to \gamma\chi_{c2}, \chi_{c2} \to p\bar{n}\pi^-$ are estimated to be about 3.4%, 4.0%, 12%, 14%, and 25%, respectively, by changing the order of the background polynomial and the fitting range.

7. The effect of the requirement on the angle between the nearest neutral cluster and the missing momentum direction of all charged tracks is checked with $J/\psi \to p\bar{n}\pi^- + c.c.$ candidate events, where the statistics are much higher and the background is much lower. We require the same selection criteria on these two channels as $\psi(2S) \to p\bar{n}\pi^- + c.c.$ except for the requirement on α. By applying the requirement on α, we measure the efficiency of this selection criterion experimentally.

   The efficiency difference for $J/\psi \to p\bar{n}\pi^-$ between data and MC simulation is measured to be $\frac{\epsilon_{DT}}{\epsilon_{MC}} = (101.60 \pm 0.53)\%$. We take $f_1 = 1.02$ as the efficiency correction factor for channels containing a $\bar{n}$.

   The efficiency difference for $J/\psi \to \bar{p}n\pi^+$ is measured to be $\frac{\epsilon_{DT}}{\epsilon_{MC}} = (89.80 \pm 0.49)\%$. We take $f_2 = 0.90$ as the efficiency correction factor for channels containing a n. The big difference in the efficiency is due to the fact that the simulation of the hadronic interaction of the neutron with the detector material is not very reliable. The systematic error on the efficiency associated with this requirement is taken as 0.5% .

8. The energy observed in the BSC associated with the positive charged track is required to be less than 0.7 GeV. The effect of this selection criterion is checked with $J/\psi \to \bar{p}n\pi^+$ candidate events, the efficiency difference between data and MC simulation is measured to be $\frac{\epsilon_{DT}}{\epsilon_{MC}} = (100.21 \pm 0.27)\%$, and we take 0.5% as the systematic error on the efficiency associated with this selection criterion.

9. In order to select $\psi(2S) \to \gamma\chi_{cJ}, \chi_{cJ} \to p\bar{n}\pi^-\pi^0$, $\psi(2S) \to p\bar{n}\pi^-\pi^0$, and $\psi(2S) \to \gamma\chi_{cJ}, \chi_{cJ} \to p\bar{n}\pi^-$ candidate events, four, three, and two photons are required, respectively. The effect of these selection criteria are checked with $J/\psi \to p\bar{n}\pi^-$ candidate events, and the efficiency difference between data and MC simulation is measured to be $\frac{\epsilon_{DT}}{\epsilon_{MC}} = (93.8 \pm 2.2)\%$. Because the MC simulates less fake photons than in data. We take $f_3 = 0.94$ as the efficiency correction factor for three background channels analyzed, and take 2.4% as the systematic error on the efficiencies associated with these three selection criteria.

Table I lists all the systematic errors, and the total systematic errors for $\psi(2S) \to p\bar{n}\pi^-$, $\psi(2S) \to \bar{p}n\pi^+$, $\psi(2S) \to p\bar{n}\pi^-\pi^0$, $\psi(2S) \to \gamma\chi_{c0}$, $\chi_{c0} \to p\bar{n}\pi^-$, and $\psi(2S) \to \gamma\chi_{c2}$,

$\chi_{c2} \to p\bar{n}\pi^-$ are 8.4%, 8.6%, 16%, 17%, and 27%, respectively. The systematic error for $\psi(2S) \to \gamma\chi_{cJ}$, $\chi_{cJ} \to p\bar{n}\pi^-\pi^0$ is 11%.

TABLE I: Summary of systematic errors (%), the errors common to all modes are only listed once, and "$\cdots$" means no contribution.

Source	$p\bar{n}\pi^-$	$\bar{p}n\pi^+$	$\gamma\chi_{cJ} \to \gamma p\bar{n}\pi^-\pi^0$	$p\bar{n}\pi^-\pi^0$	$\gamma\chi_{c0} \to \gamma p\bar{n}\pi^-$	$\gamma\chi_{c2} \to \gamma p\bar{n}\pi^-$
MC statistics	0.6	0.5	2.3	2.3	2.0	1.8
1C kinematic fit	$\cdots$	$\cdots$	4.0	4.0	4.0	4.0
Photon efficiency	$\cdots$	$\cdots$	6.0	4.0	2.0	2.0
Fitting	3.4	4.0	$\cdots$	12	14	25
E_+	$\cdots$	0.5	$\cdots$	$\cdots$	$\cdots$	$\cdots$
N_γ	$\cdots$	$\cdots$	2.4	2.4	2.4	2.4
Tracking error				4.0		
$\lvert V_z^+ - V_z^- \rvert$				0.6		
PID efficiency				5.0		
α				0.5		
$N_{\psi(2S)}$				4.0		
Sum	8.4	8.6	11	16	17	27

VI. RESULTS AND DISCUSSION

For the signal channel $\psi(2S) \to p\bar{n}\pi^- + c.c.$, the branching fractions of the main background channels are given above. From the inclusive and exclusive MC simulations, the contributions of other background channels in the missing mass distributions of $p\pi^-$ and $\bar{p}\pi^+$ show no peak. By fitting the missing mass distributions of $p\pi^-$ and $\bar{p}\pi^+$ with signal histograms obtained from MC simulation, normalized histograms of the MC simulated main background channels measured in this analysis, and first order Legendre functions to describe the other backgrounds, 921 ± 40 and 914 ± 42 events are obtained. The fits are shown in Fig. 1. The efficiency for $\psi(2S) \to p\bar{n}\pi^-$ is $\epsilon_5 = (26.48 \pm 0.14)\%$, and the branching

fraction is:

$$B(\psi(2S) \to p\bar{n}\pi^-) = \frac{N^{sig}_{p\bar{n}\pi^-}}{N_{\psi(2S)} \cdot \epsilon_5 \cdot f_1} = (2.45 \pm 0.11 \pm 0.21) \times 10^{-4}.$$

The efficiency for $\psi(2S) \to \bar{p}n\pi^+$ is $\epsilon_6 = (28.83 \pm 0.15)\%$, and the branching fraction is:

$$B(\psi(2S) \to \bar{p}n\pi^+) = \frac{N^{sig}_{\bar{p}n\pi^+}}{N_{\psi(2S)} \cdot \epsilon_6 \cdot f_2} = (2.52 \pm 0.12 \pm 0.22) \times 10^{-4}.$$

Here f_1, f_2 are the correction factors to the efficiencies, and the first errors are statistical and the second ones are systematic.

Taking events with the missing mass within ± 0.1 GeV/c^2 around the neutron mass, we get 851 and 849 for $\psi(2S) \to p\bar{n}\pi^-$ and $\psi(2S) \to \bar{p}n\pi^+$ events, respectively. The Dalitz plots for these two channels, which are similar, are shown in Fig. 6. The asymmetry between $p\pi$ and $n\pi$ is partly due to the difference in detection efficiency and may be partly due to isospin symmetry breaking effects from the electromagnetic interaction [18]. From the plots, the contribution of the N^* states at around $1.4-1.5$ GeV/c^2 can be seen, and there is a possible vertical band at around $m^2 = 4.75$ (GeV/c^2)^2. A similar band in the horizontal direction is even less clear since the events on the right side, where the recoil proton (antiproton) has low momentum and cannot be detected well by the detector, have low efficiency.

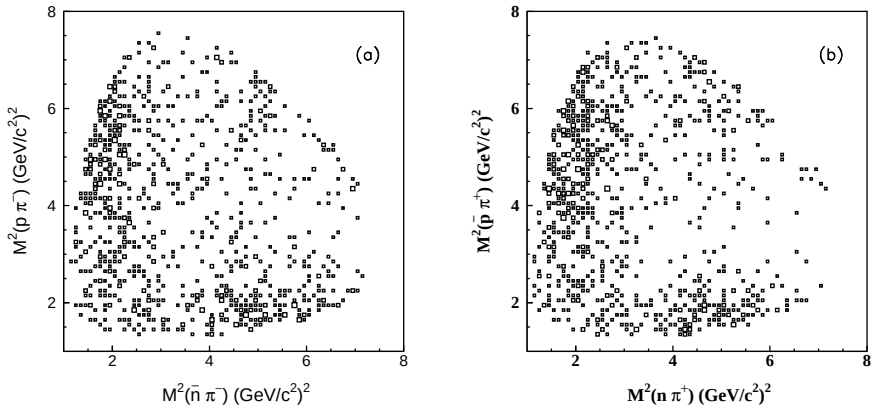

FIG. 6: Dalitz plots for (a) $\psi(2S) \to p\bar{n}\pi^-$ and (b) $\psi(2S) \to \bar{p}n\pi^+$. Here we require $|m^{recoil}_{p\pi} - 0.938| < 0.1$ GeV/c^2.

Figure 7 shows the $p\pi^-$ (or $\bar{p}\pi^+$) and $\bar{n}\pi^-$ (or $n\pi^+$) invariant mass distributions for $\psi(2S) \to p\bar{n}\pi^- + c.c.$ In order to investigate the behavior of the amplitude squared as a function of invariant mass, the invariant mass distributions are divided by phase space and

corrected by the mass dependent efficiency. The results are shown in Fig. 8. There is a large accumulation of events below 1.5 GeV/c^2, which may be due to $N^*(1440)$, $N^*(1520)$, $N^*(1535)$, etc. The cluster of events above 2 GeV/c^2 is partly due to the reflection of the $N^*(1440)$ etc., and partly may due to high mass N^* states, for example $N^*(2190)$, $N^*(2220)$, $N^*(2250)$. No clear $N^*(2065)$ peak is observed in the plots, although we can not rule out its existence. Partial wave analysis is necessary to obtain more information about the N^* components in the data. However, here the statistics are not large enough for such an analysis.

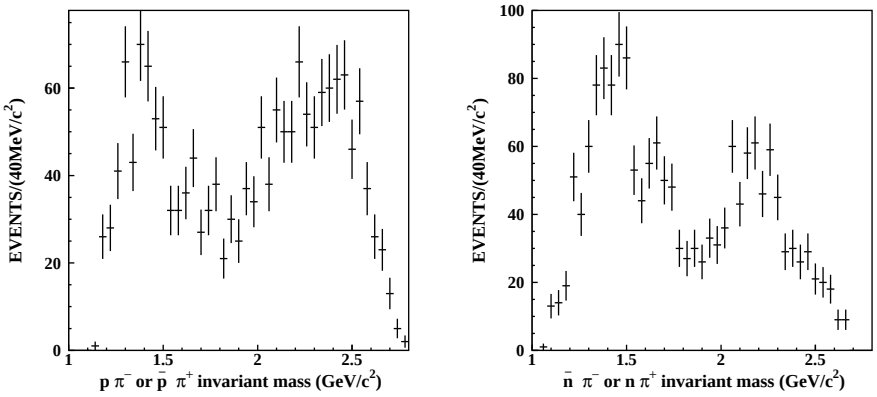

FIG. 7: $p\pi^-$ (or $\bar{p}\pi^+$) and $\bar{n}\pi^-$ (or $n\pi^+$) invariant mass distributions for $\psi(2S) \to p\bar{n}\pi^- + c.c.$

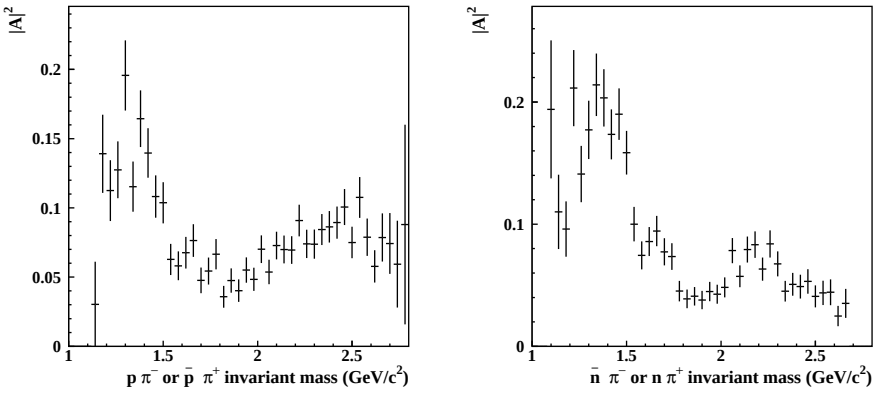

FIG. 8: Data corrected by MC simulated efficiency and phase space versus $p\pi^-$ (or $\bar{p}\pi^+$) and $\bar{n}\pi^-$ (or $n\pi^+$) invariant mass for $\psi(2S) \to p\bar{n}\pi^- + c.c.$ candidate events.

Using the J/ψ decay results in Refs. [19–21], we obtain:

$$Q_{p\bar{n}\pi^-} = \frac{B(\psi(2S) \to p\bar{n}\pi^-)}{B(J/\psi \to p\bar{n}\pi^-)} = (12.0 \pm 1.5)\%,$$

$$Q_{\bar{p}n\pi^+} = \frac{B(\psi(2S) \to \bar{p}n\pi^+)}{B(J/\psi \to \bar{p}n\pi^+)} = (12.9 \pm 1.7)\%,$$

which agree with the 12% rule within one standard deviation.

Using the branching fraction of $\psi(2S) \to p\bar{p}\pi^0$ from Ref. [12], the ratio of $B(\psi(2S) \to p\bar{p}\pi^0) : B(\psi(2S) \to p\bar{n}\pi^-) : B(\psi(2S) \to \bar{p}n\pi^+)$ is measured to be $1 : (1.86 \pm 0.27) : (1.91 \pm 0.27)$. In calculating this ratio, the common systematic errors between them have been removed. This ratio is consistent with the ratio $1 : 2 : 2$ predicted by isospin symmetry.

VII. SUMMARY

Using 14 million $\psi(2S)$ events, the branching fractions of $\psi(2S) \to p\bar{n}\pi^-$, $\psi(2S) \to \bar{p}n\pi^+$, $\psi(2S) \to p\bar{n}\pi^-\pi^0$, $\psi(2S) \to \gamma\chi_{c0}, \chi_{c0} \to p\bar{n}\pi^-$, and $\psi(2S) \to \gamma\chi_{c2}, \chi_{c2} \to p\bar{n}\pi^-$ are measured to be:

$$B(\psi(2S) \to p\bar{n}\pi^-) = (2.45 \pm 0.11 \pm 0.21) \times 10^{-4},$$

$$B(\psi(2S) \to \bar{p}n\pi^+) = (2.52 \pm 0.12 \pm 0.22) \times 10^{-4},$$

$$B(\psi(2S) \to p\bar{n}\pi^-\pi^0) = (3.18 \pm 0.50 \pm 0.50) \times 10^{-4},$$

$$B(\psi(2S) \to \gamma\chi_{c0}, \chi_{c0} \to p\bar{n}\pi^-) = (1.10 \pm 0.24 \pm 0.18) \times 10^{-4},$$

$$B(\psi(2S) \to \gamma\chi_{c2}, \chi_{c2} \to p\bar{n}\pi^-) = (0.97 \pm 0.20 \pm 0.26) \times 10^{-4},$$

where the first errors are statistical and the second are systematic. The upper limit of $\sum_{J=0}^{2} B(\psi(2S) \to \gamma\chi_{cJ}, \chi_{cJ} \to p\bar{n}\pi^-\pi^0)$ is estimated to be 1.2×10^{-4} at the 90% C. L.

Acknowledgments

The BES collaboration thanks the staff of BEPC for their hard efforts. This work is supported in part by the National Natural Science Foundation of China under contracts Nos. 10491300, 10225524, 10225525, 10425523, the Chinese Academy of Sciences under contract No. KJ 95T-03, the 100 Talents Program of CAS under Contract Nos. U-11, U-24, U-25, and the Knowledge Innovation Project of CAS under Contract Nos. U-602, U-34 (IHEP),

the National Natural Science Foundation of China under Contract No. 10225522 (Tsinghua University), and the Department of Energy under Contract No. DE-FG02-04ER41291 (U Hawaii).

---

[1] T. Appelquist and H. D. Politzer, Phys. Rev. Lett. **34**, 43 (1975); A. De Rújula and S. L. Glashow, Phys. Rev. Lett. **34**, 46 (1975).

[2] M. E. B. Franklin *et al.* (Mark-II Collaboration), Phys. Rev. Lett. **51**, 963 (1983).

[3] J. L. Rosner, Phys. Rev. D **64**, 094002 (2001).

[4] P. Wang, C. Z. Yuan and X. H. Mo, Phys. Rev. D **70**, 114014 (2004).

[5] Proceedings of the Workshop on the Physics of Excited Nucleons, (NSTAR2002) eds. S. A. Dytman and E. S. Swanson, World Scientific, 2003; (NSTAR2001) eds. D. Drechsel and L. Tiator, World Scientific, 2001.

[6] M. Ripani *et al.*, Phys. Rev. Lett. **91**, 022002 (2003); S. Stepanyan *et al.*, Phys. Rev. Lett. **91**, 252001 (2003).

[7] T. Nakano *et al.*, Phys. Rev. Lett. **91**, 012002 (2003).

[8] S. Eidelman *et al.* (Particle Data Group), Phys. Lett. B **592**, 1 (2004).

[9] S. Capstick and W. Roberts, Prog. Part. Nucl. Phys. **45**, S241 (2000).

[10] B. S. Zou, Nucl. Phys. A **675**, 167C (2000).

[11] M. Ablikim *et al.* (BES Collaboration), hep-ex/0405030.

[12] M. Ablikim *et al.* (BES Collaboration), Phys. Rev. D **71**, 072006 (2005).

[13] J. Z. Bai *et al.* (BES Collaboration), Nucl. Instrum. Methods Phys. Res., Sect. A **458**, 627 (2001).

[14] M. Ablikim *et al.* (BES Collaboration), Nucl. Instrum. Methods Phys. Res., Sect. A **552**, 344 (2005).

[15] X. H. Mo *et al.*, High Energy Phys. Nucl. Phys. **28**, 455 (2004). [hep-ex/0407055].

[16] J. C. Chen, G. S. Huang, X. R. Qi, D. H. Zhang and Y. S. Zhu, Phys. Rev. D **62**, 034003 (2000).

[17] M. Ablikim *et al.* (BES Collaboration), Phys. Rev. D **70**, 112007 (2004).

[18] L. Köpke and N. Wermes, Phys. Rept. **174**, 67 (1989).

[19] M. W. Eaton *et al.*, Phys. Rev. D **29**, 804 (1984).

[20] H. J. Besch *et al.*, Z. Phys. C **8**, 1 (1981).

[21] I. Peruzzi, M. Piccolo *et al.*, Phys. Rev. D **17**, 2901 (1978).